https://doi.org/10.5194/egusphere-2026-5294
Preprint. Discussion started: 16 November 2026
© Author(s) 2026. CC BY 4.0 License.

Quantifying methane emissions of the oil and gas sector in the Sultanate of Oman based on a helicopter-borne mass balance approach

Eric Förster[1], Heidi Huntrieser[1], Niclas Maier[1], Halima Al Hinaai[1], Benjamin Witschas[1], Falk Pätzold[2], Lutz Bretschneider[2], Sven Bollmann[2], Andreas Schlerf[2], Astrid Lampert[2], Jaroslaw Necki[3], Pawel Jagoda[3], Jakub Bartyzel[3], Mark Lunt[4], Mohammed Ajmi[5], Nabil Al Lawati[5], Ahmed Abri[5], and Anke Roiger[1]

[1]DLR – Deutsches Zentrum für Luft- und Raumfahrt, Institute of Atmospheric Physics, Oberpfaffenhofen, Germany
[2]TUB – Technische Universität Braunschweig, Institute of Flight Guidance, Braunschweig, Germany
[3]AGH – University of Kraków, Faculty of Physics and Applied Computer Science, Kraków, Poland
[4]EDF – Environmental Defense Fund, Perth, Australia
[5]Industrial Partner, Sultanate of Oman

Correspondence to: Eric Förster (Eric.Foerster@dlr.de) and Heidi Huntrieser (Heidi.Huntrieser@dlr.de)

Abstract

Methane (CH_4) emissions from the oil and gas (O&G) sector remain poorly constrained across the Arabian Peninsula. We present the first airborne quantification of O&G CH_4 emissions in Oman, conducted in 2023 with the helicopter-towed *HELiPOD*, ground surveys, and satellite observations.

Airborne estimates ranged from 60 to 2200 kg h^{-1} for sweet facilities and facility clusters. At sour facilities handling sulfur- and/or CO_2-rich streams, all estimates remained below the *HELiPOD* quantification threshold of approximately 16 kg h^{-1}. Ground surveys corroborated this contrast, showing fewer leaks and less frequent small enhancements around sour facilities. Ground and satellite observations identified a maintenance-related super-emitting event, while *HELiPOD* validated these observations and quantified dispersed sources not resolved by satellite observations. Top-down and operator-provided bottom-up estimates were comparable in magnitude for individual facilities but differed sevenfold for a complex cluster because the bottom-up estimate missed the event.

The marketed O&G-production-normalised loss rate was 0.20 ± 0.07 % (0.58 ± 0.26 % relative to marketed gas), below most Oman inventory estimates (0.3 to 2.5 %) but about seven times the operator estimate of 0.03 %. Excluding the event yielded 0.12 ± 0.07 %. Loss rates were also lower than reported for the United States, Canada, and Turkmenistan (0.3 to 3.2 %).

Low sour-facility CH_4 emissions suggest that controls required for safe H_2S handling, including tightly sealed infrastructure, also limit CH_4 emissions and demonstrate the feasibility of comparable mitigation controls elsewhere. Coordinated multi-scale observations can constrain inventories, capture diffuse and non-routine emissions, and guide targeted mitigation.

1 Introduction

With a 20-year global warming potential, approximately 80 times higher than that of carbon dioxide (CO_2), methane (CH_4) is the second most important anthropogenic greenhouse gas (GHG), and its impact on climate change is well documented (Kirschke et al., 2013; Forster et al., 2021). Due to its comparatively short atmospheric lifetime (~9 years), rapid reductions in CH_4 emissions can have a more immediate climate benefit than comparable reductions in CO_2 emissions. Highly emissive sectors such as coal mining, waste management, livestock cultivation, and particularly oil and gas (O&G) production contribute substantially to global anthropogenic CH_4 emissions (Saunois et al., 2020). In this study, we focus on the O&G sector.

In 2023, global oil production reached approximately 82 million barrels per day (EIA, 2025), while natural gas production amounted to 4,143 billion cubic metres, equivalent to approximately 67 million barrels of oil equivalent (BOE) per day. The

https://doi.org/10.5194/egusphere-2026-5294
Preprint. Discussion started: 16 November 2026
© Author(s) 2026. CC BY 4.0 License.

Arabian Peninsula (AP, including Bahrain, Kuwait, Oman, Qatar, Saudi Arabia, United Arab Emirates, and Yemen) is a major contributor to these production volumes. Saudi Arabia, the United Arab Emirates (UAE), and Qatar together account for approximately 22 % of global oil and 10 % of global gas production.

O&G production is associated with substantial CH_4 emissions worldwide. The International Energy Agency (IEA, 2024) estimated global O&G-related CH_4 emissions at approximately 80 Mt in 2023, corresponding to 22 % of total anthropogenic CH_4 emissions (Saunois et al., 2025). At the global scale, satellite-based estimates further indicate that O&G-related CH_4 emissions may be approximately 30 % higher than reported in national bottom-up inventories, with particularly large discrepancies for several major producing countries (Shen et al., 2023). Recent studies of CH_4 emissions in the Middle East similarly report substantial discrepancies between observed and inventory-based estimates across different sectors (Paris et al., 2021; Bourtsoukidis et al., 2024; Gasim et al., 2024; Germain-Piaulenne et al., 2024; Liu et al., 2024). Oil-related CH_4 emissions in the northern Arabian Gulf may be underestimated, whereas gas-related emissions in the southern Gulf may be overestimated compared with inventories (Paris et al., 2021). Other studies suggest that O&G-related CH_4 emissions in the Middle East are underestimated by up to 69 % (Germain-Piaulenne et al., 2024), while discrepancies between satellite-based estimates and inventory products vary strongly among countries (Gasim et al., 2024).

For the Arabian Peninsula, available inventories and satellite-based estimates differ substantially, ranging from 2.2 to 8.9 Mt yr^{-1} for the region (Fig. 1; Table S1 and S2). Figure 1 illustrates these discrepancies across the Arabian Peninsula. While year-to-year variability within individual inventories is comparatively small, the spread among inventories for individual countries, expressed as the relative standard deviation of the estimates shown in Fig. 1, ranges from 22 % for Saudi Arabia to 69 % for Yemen, with a value of 54 % for Oman. However, most previous studies in the region relied primarily on satellite observations or far-field atmospheric measurements outside of the Arabian Peninsula and thereby requiring the use of long-range transport and inverse modelling approaches. Consequently, targeted in-country field campaigns and long-term observations are required to improve the understanding of complex O&G-related CH_4 emissions in the Middle East and to provide independent validation opportunities for inventories and satellite retrievals.

Oman represents a particularly relevant case study because, despite contributing only approximately 1 % of global O&G production, reported CH_4 emissions from the O&G sector differ strongly between inventories, satellite products, and national reporting. First estimates of CH_4 emissions from the O&G sector ranged from approximately 565 kt in 2010 (Albusaidi, 2019) to 634 kt in 2015 (Charabi, 2021), whereas more recent inventory- and satellite-based estimates range from 237 to 2318 kt yr^{-1} (Fig. 1). In comparison, the First Biennial Transparency Report of the Sultanate of Oman to the United Nations Framework Convention on Climate Change (UNFCCC) reported CH_4 emissions from the energy sector of only 130 kt in 2022.

Al-Shidhani and Hayyan (2025) further reported that greenhouse gas emissions associated with Oman's natural gas sector increased strongly from approximately 12 Mt CO_2 in 2000 to around 50 Mt CO_2 in 2020. In response to the growing importance of fossil-related greenhouse gas emissions, Oman joined the Global Methane Pledge (https://www.globalmethanepledge.org, last access: 27 August 2026) with the target to reduce CH_4 emissions by 30 % between 2020 and 2030 and established a net-zero target for 2050. Ensuring the integrity of such mitigation commitments requires independent atmospheric observations and verification measurements (Nisbet and Weiss, 2010), particularly in regions where large discrepancies exist between inventories, satellite observations, and reported emissions. In this context, the United Nations Environment Programme (UNEP) supports CH_4 monitoring through the International Methane Emissions Observatory (IMEO, 2024), including the Oil and Gas Methane Partnership 2.0 (OGMP 2.0), a voluntary measurement-based reporting framework for the O&G sector. These developments provide an important framework and motivation for independent multi-scale CH_4 observations in Oman.

https://doi.org/10.5194/egusphere-2026-5294
Preprint. Discussion started: 16 November 2026
© Author(s) 2026. CC BY 4.0 License.

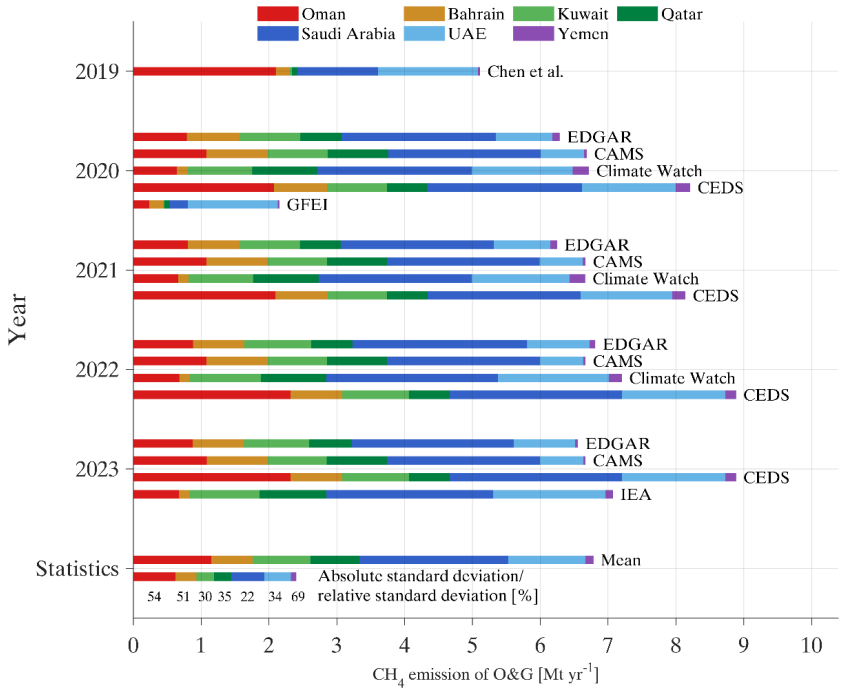


Figure 1. Overview of CH_4 emissions [Mt yr^{-1}] from the oil and gas sector of the Arabian Peninsula (status 2023), based on a satellite-derived estimate (Chen et al., 2023) and different bottom-up inventories (EDGAR - Emissions Database for Global Atmospheric Research, CAMS - Copernicus Atmosphere Monitoring Service, Climate Watch, CEDS - Community Emissions Data System, GFEI - Global Fuel Exploitation Inventory, IEA - International Energy Agency, see Tables S1 and S2 for more information). Chen et al. (2023) provide estimates for 2019 based on TROPOMI satellite data. For the five years, mean and standard deviations (STD) for the respective countries are given. The percentages give the relative STD.

Methane emissions from the O&G sector represent a highly complex and variable emission landscape, characterised by strong temporal variability, large differences between facilities, and a wide range of emission magnitudes. Previous studies have suggested that CH_4 emissions from some O&G production regions follow strongly skewed, heavy-tailed distributions, in which a small fraction of sites or events dominates total emissions at facility or basin scales (e.g. Frankenberg et al., 2016; Duren et al., 2019; Esparza et al., 2023; Sherwin et al., 2024). In recent satellite-based studies, emissions exceeding approximately 500 kg CH_4 h^{-1} have commonly been considered satellite-detectable "super-emitters" (Irakulis-Loitxate et al., 2021; Huang et al., 2026). Across different O&G production regions, approximately 1 to 12 % of emitting sources were found to account for 40 to 80 % of total CH_4 emissions, often driven by short-lived super-emitter events associated with tank venting, abnormal venting, flaring inefficiencies, and equipment malfunctions (e.g. Zavala-Araiza et al., 2017; Alvarez et al., 2018; Irakulis-Loitxate et al., 2021; Johnson et al., 2023; O'Callaghan, 2024). At the same time, the apparent emission distribution may partly depend on the applied measurement approach, as methods optimised for detecting large point sources may not capture the full spectrum of smaller, spatially distributed emissions. Such smaller but persistent sources can nevertheless contribute substantially to total facility- or cluster-scale CH_4 emissions (Williams et al., 2025). These findings suggest that the relative importance of super-emitters and diffuse emissions may vary considerably between production regions, highlighting the need for basin-specific observations.

In addition to operational conditions and non-routine emission events, including equipment malfunctions and abnormal venting, infrastructure characteristics may also influence CH_4 emissions. In O&G production, "sweet" facilities process

https://doi.org/10.5194/egusphere-2026-5294
Preprint. Discussion started: 16 November 2026
© Author(s) 2026. CC BY 4.0 License.

hydrocarbons with negligible sulfur and CO_2 content, whereas "sour" facilities handle streams containing elevated concentrations of sulfur compounds such as hydrogen sulfide (H_2S), requiring gas sweetening systems, corrosion-resistant infrastructure, and stricter safety controls (Roscioli et al., 2015; Natural Gas.Org, 2025). Previous studies suggest that stricter operational requirements and mitigation measures associated with sour gas handling contribute to lower CH_4 emissions in these regions (Lavoie et al., 2022).

These intermittent and spatially heterogeneous emissions are difficult to represent in bottom-up approaches, which include company-reported emission factors and inventories relying primarily on engineering estimates and limited observational constraints. Top-down estimates are instead derived from atmospheric observations at different spatial scales, including ground-based, drone-based, airborne, and spaceborne (satellite) observations of CH_4 emissions. The overarching goal of using diverse measurement approaches is therefore to reconcile discrepancies between bottom-up and top-down CH_4 emission estimates (Nisbet and Weiss, 2010; Brandt et al., 2014; Allen, 2016; Petrescu et al., 2024; Barkley et al., 2025).

Each observational platform provides specific advantages and limitations. Ground-based measurements provide detailed source attribution and identification of individual leakages but are generally less efficient at covering large areas than airborne or satellite observations and do not constrain integrated facility-scale emissions. Satellite observations from area flux mappers such as TROPOMI and GOSAT and point-source imagers such as PRISMA, EMIT, and the GHGSat constellation provide regional to global coverage and are highly effective for detecting major super-emitting events. However, satellite detection thresholds remain strongly dependent on surface reflectance, cloud cover, wind speed, and viewing geometry (Jacob et al., 2016; Gorroño et al., 2023; McLinden et al., 2024), while smaller and spatially diffuse emissions are often not resolved. Despite these limitations, recent EMIT and PRISMA observations identified multiple super-emitting CH_4 plume events in Oman between 2020 and 2023 (Huang et al., 2026), highlighting the importance of targeted follow-up observations.

Airborne measurements provide an observational bridge between localised ground-based surveys and large-scale satellite observations by integrating emissions across entire facilities or production regions while maintaining direct proximity to emission sources. While fixed-wing aircraft can efficiently cover large areas, helicopter-borne sensing platforms offer greater manoeuvrability and operational flexibility, enabling low-altitude measurements and repeated plume transects close to complex emission sources. Previous studies demonstrated that the helicopter-towed *HELiPOD* platform can detect CH_4 emissions as low as 20 kg h^{-1} and accurately quantify emissions from complex industrial sources, including coal mine ventilation shafts in Poland (Förster et al., 2025). In addition, helicopter-based measurements are logistically advantageous in regions with limited access for foreign research aircraft. Collaborating with local helicopter operators and operating the *HELiPOD* as an external sling load enables flexible deployments, avoids the need for dedicated aircraft certification, and facilitates the acquisition of local flight permissions.

Against this background, we conducted the first airborne quantification of CH_4 emissions on the Arabian Peninsula during the five-week METHANE-To-Go-Oman campaign in November and December 2023. As discussed above, Oman represents a particularly relevant case study due to the large uncertainties in reported CH_4 emissions, the increasing interest in CH_4 mitigation and monitoring initiatives, and the strong interest of national stakeholders in independent atmospheric CH_4 observations.

In this study, we combine helicopter-borne *HELiPOD* observations with mobile ground-based CH_4 measurements to investigate CH_4 emissions from individual O&G facilities and industrial clusters across different production regions in Oman. The measurements were designed to characterise complex emission landscapes, investigate the complementarity of airborne, ground-based, and satellite observations, and provide independent validation opportunities for source-level CH_4 emission estimates. Section 2 describes the applied measurement systems and emission quantification methods. Results and discussion are presented in Sect. 3 and 4, respectively, followed by summary and conclusions in Sect. 5.

https://doi.org/10.5194/egusphere-2026-5294
Preprint. Discussion started: 16 November 2026
© Author(s) 2026. CC BY 4.0 License.

2 Methodology

This section first describes the campaign design, target selection, and flight operations (Sect. 2.1), followed by the *HELiPOD* platform and instrumentation (Sect. 2.2). We then present the airborne sampling strategy and mass-balance approach (Sect. 2.3), before describing the complementary mobile ground-based measurements (Sect. 2.4) and the calculation of production-normalised CH_4 loss rates (Sect. 2.5).

2.1 The METHANE-To-Go-Oman campaign

During the METHANE-To-Go-Oman campaign (MTG-Oman), we conducted the first airborne GHG measurements on the Arabian Peninsula, specifically over the Sultanate of Oman. Previous airborne studies in this region are very sparse and date back roughly two decades, focusing mainly on aerosol properties (Reid et al., 2008). For the present study, the innovative helicopter-towed probe *HELiPOD* was deployed (Pätzold et al., 2023), carried by an Airbus H125 (Fig. 2) from a local helicopter company.



Figure 2. The helicopter-borne measurement system *HELiPOD* with its carrier, an Airbus H125 from the Omani company Al Sharqiya Aviation (ASA).

The campaign included 22 *HELiPOD* mission flights targeting O&G infrastructure, with an average duration of 2.5 h, conducted in three regions in the northern and southern parts of the Sultanate of Oman (Regions A, B, and C, respectively) between 14 November and 9 December 2023. The measurements covered six different O&G assets (see Table S3), anonymised in this study as Targets 1 to 6. Each individual target in Regions A-C comprised one or more centralised facilities (e.g. a gas processing facility) surrounded by tens to hundreds of wells and the associated pipeline network. More precise information on the locations and identities of the investigated regions and facilities is not provided due to the operator's confidentiality requirements.

Target selection was primarily constrained by campaign logistics. The investigated facilities had to be located within an operational radius of approximately 150 km from a suitable airfield that could serve as a temporary campaign base. Within these constraints, the selected targets were chosen to cover a range of facility characteristics, including sweet and sour production, facilities of different ages, and both individual assets and larger industrial clusters. The campaign was intended as a first targeted airborne investigation of O&G-related CH_4 emissions in Oman rather than as a statistically representative survey of national production.

The facility operators were closely involved in the logistical and operational planning of the campaign. As several target regions were located in remote desert areas, the operators also supported local accommodation and access arrangements. Planned target areas and flight schedules were generally communicated approximately three days in advance, including the

https://doi.org/10.5194/egusphere-2026-5294
Preprint. Discussion started: 16 November 2026
© Author(s) 2026. CC BY 4.0 License.

expected measurement times. This advance notice was required for flight coordination and site safety, particularly to inform personnel working near the facilities about the low-altitude helicopter operations and the externally suspended *HELiPOD*. Apart from occasional short delays related to local air traffic, the measurements could generally be conducted according to the planned schedule.

2.2 The *HELiPOD* platform and used instrumentation

The *HELiPOD* is a helicopter-towed measurement platform designed for environmental and atmospheric research, limited in flight time and mission distance by the helicopter capabilities, typically 2.5 hours and 350 line km. In Oman typical deployment altitudes have been between 30 m above ground and 3000 m above mean sea level. Measuring 5.2 m x 2.1 m x 1.2 m and weighting about 325 kg, including payload, the *HELiPOD* is powered by one or two 5 kWh batteries, allowing it to operate independently from the towing helicopter. The design of the *HELiPOD* and the typical helicopter speed of 40 m s^{-1} ensure that, during cruise flight, the rotor wake of the helicopter (downwash) does not interfere with the *HELiPOD's* measurements, as the downwash is almost horizontally oriented (see Pätzold et al., 2023 and Förster et al., 2025).

For the MTG-Oman campaign, the scientific payload included instruments to measure the greenhouse gases CH_4 (the main focus of this study) and CO_2, the short-lived trace gas sulfur dioxide (SO_2), and meteorological parameters. CO_2 and SO_2 will be analysed in separate studies. Two in situ CH_4 analysers were used: the cavity ring-down spectroscopy-based Picarro G2401-m (Crosson, 2008; Klausner et al., 2020) installed inside the *HELiPOD*, and the open-path Licor LI-7700 (McDermitt et al., 2011) mounted externally. Each system offered distinct measurement capabilities - Picarro with higher precision up to 1 ppb and Licor with higher sampling frequency up to 40 Hz (for details on the instrumentation, see Table S4 and Förster et al., 2025). Calibrations were performed every two to three days using three different NOAA (National Oceanic and Atmospheric Administration) corrected Air Liquide standards with high (2690 ppb), middle (1845 ppb) and low (1625 ppb) mixing ratios to ensure data quality.

The 3D wind vector was derived by subtracting the airspeed (measured using a five-hole probe) from the groundspeed, determined using a Global Navigation Satellite System aided inertial measurement unit system (GNSS-IMU-System), for more details see Pätzold et al. (2023). Temperature and humidity data were measured using several sensors with different physical measuring principles and different transfer behaviours regarding measurement dynamics. As fast sensors tend to drift in time while slow sensors are more stable, the postprocessing using complementary filtering in frequency domain delivers broadband drift-free data (Pätzold et al., 2023). All sensor data are either recorded at their intrinsic data rate or sampled with 100 Hz, precisely time-stamped and stored onboard for post-processing, which included applying calibration factors and corrections, particularly for wind vector measurements.

2.3 Mass balance approach and sampling strategy

We use a mass balance approach to estimate CH_4 mass fluxes of selected O&G facilities. This approach is described in detail elsewhere (e.g. Cambaliza et al., 2014; Conley et al., 2017) and was recently applied for *HELiPOD* measurements in Poland (Förster et al., 2025). Briefly, the mass flux F of a species C through a crosswind curtain downwind is estimated by the integration of the enhancement above the background concentration $[C]_{bg}$ combined with the wind speed component of the wind $U_\perp$ perpendicular to the curtain, following Eq. 1:

$$F = \int_{Z_0}^{Z_{PBL\,top}} \int_{-x}^{x} \left([C] - [C]_{bg}\right) U_\perp \, dx \, dz \tag{1}$$

https://doi.org/10.5194/egusphere-2026-5294
Preprint. Discussion started: 16 November 2026
© Author(s) 2026. CC BY 4.0 License.

The parameters z_0 and z_{PBLtop} are the vertical limits of the plume from ground to the top of the convective planetary boundary layer (PBL) and -x and +x are the horizontal limits of the plume width from an arbitrary midpoint (Cambaliza et al., 2014). The PBL height and also inversion layer(s) are derived from measured vertical *HELiPOD* profiles of the potential temperature (θ) and its gradient $d\theta\ dz^{-1}$, H_2O and CH_4 concentrations (e.g. Cambaliza et al., 2014; Dai et al., 2014), taken at the beginning and end of each individual flight up to an altitude of 3 km. The brackets around the trace species *C* denote the measured concentration. Full integration over the limits of the plane yields an emission rate *F*, in the unit kg h^{-1}. Conventional aircraft-based mass balance studies commonly sample sufficiently far downwind for the plume to be assumed vertically well mixed within the PBL (e.g. Cambaliza et al., 2014; Conley et al., 2017; Pühl et al., 2024) . For the investigated O&G regions, however, sampling farther downwind would have increased the overlap of plumes from numerous closely spaced CH4 sources and impeded their attribution to individual facilities or facility clusters. We therefore sampled closer to the sources and explicitly resolved the vertical plume structure using stacked transects. Measurements were preferentially conducted during the comparatively stable morning period, representing the earliest suitable daylight conditions and limiting turbulence-induced plume variability, consistent with the simulations of Wolff et al. (2021) discussed below. At these shorter sampling distances, the plumes did not necessarily extend to the PBL top or even to an inversion layer (see Table S5).

We apply a discrete approach of Eq. 1 by calculating the mass flux for pointwise CH_4 enhancements during individual transects crossing the plume(s) at different altitudes downwind of the targeted emission source. The background concentration $[CH_4]_{bg}$ is individually calculated for each transect by interpolating between 10 s averages of both edges of a transect to account for gradients in the background. Methane plumes are identified by $[C\text{-}C_{bg}] + 3\sigma$, where σ is the mean of the standard deviations of the 10 s average periods at both edges. The vertical plume extension is estimated to reach the ground if no mobile ground-based transect is available and halfway up from the highest transect with enhancement to the next higher transect. If a mobile ground-based transect is available, the CH_4 enhancements at the ground and the lowest transect are estimated to reach halfway up and down, respectively. If CH_4 enhancements at the highest probed transect are still present, they are estimated to reach to the top of the PBL/inversion layer.

The total mass flux uncertainty, F_{unc} , is calculated as

$$F_{unc} = F_{unc,flux} + F_{unc,bottom} + F_{unc,top}, \quad (2)$$

and thus consists of three components: $F_{unc,flux}$ denotes the uncertainty of the flux calculation obtained by Gaussian error propagation, $F_{unc,bottom}$ denotes the uncertainty resulting from extrapolation between the lowest airborne transect and the ground, and $F_{unc,top}$ denotes he uncertainty resulting from extrapolation between the highest plume transect and the estimated plume top. The instrumental and meteorological uncertainties considered in the Gaussian error propagation are summarised in Table 1.

For F_{unc_flux}, uncertainties in CH_4 enhancement, perpendicular wind speed, pressure, temperature, and plume width were propagated through the mass balance equation. For each input parameter, where both an instrumental uncertainty and an estimate of the variability within the selected plume transect were available, the larger of the two values was used in the error propagation. The uncertainties associated with the lower and upper plume boundaries were calculated separately from the corresponding vertical extrapolation distances. We use this conservative uncertainty approach due to the closer probing to emission sources where the plume is not necessarily well mixed throughout the PBL. A detailed assessment of the mass flux uncertainty and calculation steps of the emission estimates are provided in Förster et al. (2025).

https://doi.org/10.5194/egusphere-2026-5294
Preprint. Discussion started: 16 November 2026
© Author(s) 2026. CC BY 4.0 License.

Table 1. Overview of the uncertainty components considered in the Gaussian error propagation of the *HELiPOD* mass balance flux calculations. Where applicable, the larger value of the instrumental uncertainty and the observed variability within the selected plume transect was used. The latter was quantified by the root-mean-square error (RMSE).

Uncertainty source	Value or estimation	Treatment in flux calculation
CH_4 enhancement, (ΔCH_4)	Picarro precision: 2 ppb at 2 Hz; alternatively, RMSE of the 10s background intervals, whichever was larger	Included in F_{unc_flux}; instrumental uncertainty was applied to both measured and background CH_4
Wind speed, (FF)	0.1 m s^{-1}	Propagated into the uncertainty of the perpendicular wind component $U_\perp$
Wind direction, (DD)	3°	Propagated into the uncertainty of $U_\perp$
HELiPOD heading, (HH)	RMSE during the selected plume transect	Propagated into the uncertainty of $U_\perp$
Pressure, (p)	5 Pa or transect RMSE, whichever was larger	Included in F_{unc_flux}
Temperature, (T)	0.1 K or transect RMSE, whichever was larger	Included in F_{unc_flux}
Plume width, (dx)	Derived from the RMSE of the *HELiPOD* velocity within the plume transect	Included in F_{unc_flux}

In addition to the uncertainty of individual mass flux estimates, we derived an empirical quantification threshold for the airborne mass-balance approach by applying the complete flux calculation to source-free upwind transects. Based on the 95th percentile of the resulting null-flux distribution, the campaign-specific estimate was approximately 11 kg h^{-1}, while the upper limit of the cluster-bootstrap 95 % confidence interval yielded a conservative threshold of approximately 16 kg h^{-1}. Details of the method, assumptions, and limitations are provided in Sect. S2 with Figs. S1 and S2.

The measurement flights were conducted during suitable meteorological conditions, i.e. a stably stratified atmosphere with wind speed between 3 and 10 m s^{-1}, where the emissions are advected along the prevailing wind direction and theoretically form a cone shape broadening with distance from the source. A scheme of a typical flight pattern is shown in Fig. 3. Straight race tracks with a length of around 3 to 20 km, depending on the size of the industrial cluster, were flown perpendicular to the wind direction at different altitudes downwind of the target to sufficiently capture the vertical and horizontal dimensions of the plume(s), as well as the CH_4 background concentration at both edges of the transects.

The transects were conducted at altitudes ranging from the lowest safe flight level (~50 m) up to levels where no further CH_4 enhancements were detected (up to 1600 m). If enhancements were still observed at the highest transect, the vertical extent of the plume was determined based on the observed vertical layering from the flown profiles, with interpolation applied either up to the PBL or the inversion layer (see Förster et al., 2025). Depending on the plume height, between 7 and 13 plume transects were flown per curtain with vertical intervals between 25 m and 200 m. Whenever possible, flights were conducted in the morning, approximately 1 h after sunrise, when horizontal winds had developed but the atmosphere was still comparatively stable and the inversion layer or PBL top remained at relatively low altitudes, typically below 500 m. Later in the day, the onset of convection frequently weakened and eventually suppressed the horizontal transport, while vertical transport and multidirectional turbulent dispersion became increasingly dominant. Under such conditions, the plume cross-section required for mass balance quantification could no longer be reliably captured by downwind transects because vertical transport and multidirectional turbulent dispersion dominated, as illustrated by the simulations shown in Fig. A2 of Wolff et al. (2021). For every target we conducted at least two mission flights with 1 up to 3 downwind mass balance experiments (MBE) at distances of 1 km to 10 km from the emission source (see Table S5 for details). Emissions of individual facilities were usually probed with two MBEs (min. distance 1 km to separate nearby sources, max. distance 4 km), emissions of facility clusters with one MBE (min. distance 3 km, max. distance 10 km).

https://doi.org/10.5194/egusphere-2026-5294
Preprint. Discussion started: 16 November 2026
© Author(s) 2026. CC BY 4.0 License.

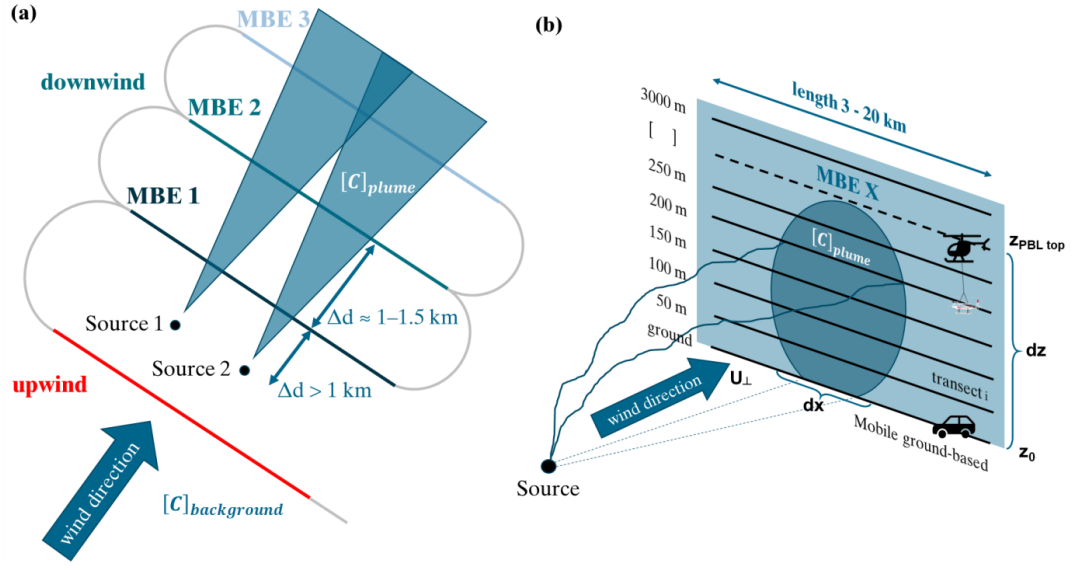


Figure 3. Scheme of the mass balance approach. (a) Example of a typical planned mass balance experiment (MBE), comprising an upwind leg (red line) to determine the background concentration $[C]_{background}$, and several downwind measurement curtains (blue lines) at increasing distances from the selected sources. (b) Structure of an individual measurement curtain composed of vertically stacked horizontal transects between the lower integration boundary z_0 and the top of the planetary boundary layer, $z_{PBL\ top}$. The horizontal and vertical integration increments are denoted by dx and dz, respectively; $U_\perp$ represents the wind component perpendicular to the curtain, and $[C]_{plume}$ denotes the plume concentration enhancement.

2.4 Ground-based measurements

HELiPOD observations were complemented by mobile ground-based CH_4 measurements (see Jagoda et al., 2024 for details), which were used to constrain the lower part of the mass balance curtains below approximately 100 m, an altitude range that was mostly inaccessible to direct *HELiPOD* sampling because of safety constraints imposed by power lines and elevated facility infrastructure. The 1 Hz CH_4 measurements were performed from a car equipped with a Licor 7810 and synchronised with GPS data. The mobile ground-based data were included in the mass-flux estimates (see Sect. 2.3 and Förster et al., 2025), if they provided a complete transect through the CH_4 plume and were spatially close to the *HELiPOD* flight tracks (mean distance < 1000 m). Ground-based measurements could be incorporated into 11 of the 35 conducted MBEs, corresponding to 7 of the 22 flights. In most cases, the latest included ground-based transect was conducted within 2 h after take-off and therefore within the typical duration of a *HELiPOD* flight of approximately 2 to 3 h. In two cases, the respective ground-based measurements were conducted approximately 4 h before and 7 h after take-off; however, flux estimates calculated with and without the ground-based data differed only marginally.

2.5 Loss rate and production estimates

To compare CH_4 emissions across O&G-producing regions with different production volumes, emission estimates are commonly normalised to hydrocarbon production (e.g. Alvarez et al., 2018). Several related terms are used in the literature for such production-normalised metrics: (i) loss rate, (ii) CH_4 intensity (Chen et al., 2023; Conrad et al., 2023) and (iii) leakage rate (Schneising et al., 2020). CH_4 emissions are e.g. normalised to combined oil and gas production, where the gas production and emissions are converted to barrels of oil equivalent (BOE, e.g. Naus et al., 2023) or to the total delivered energy in

https://doi.org/10.5194/egusphere-2026-5294
Preprint. Discussion started: 16 November 2026
© Author(s) 2026. CC BY 4.0 License.

g CH_4 MJ^{-1} (Conrad et al., 2023). With the latter metrics, the terms energy loss rate (Schneising et al., 2020) or joule loss rate (Ayasse et al., 2022) are used as well.

We define the loss rate as upstream O&G emissions per unit of marketed O&G production for the investigated assets. Because half of the targeted assets produce oil only, emissions are primarily normalised to total marketed O&G production. For completeness, gas-production-normalised loss rates are additionally provided in Supplement S4 to facilitate comparison with studies and reporting frameworks based on gas production only. Loss rates are typically expressed as a percentage, representing the mass of CH_4 emitted relative to the hydrocarbon production used for normalisation. A relevant benchmark is the Oil and Gas Climate Initiative (OGCI) target of 0.2 % for upstream CH_4 emissions by 2025, expressed as a CH_4 loss rate normalised to marketed gas production rather than total O&G production (OGCI, 2025).

We used production data from two sources, Rystad (Rystad, 2024 data, https://www.rystadenergy.com/, last access 27 August 2026) and Wood Mackenzie (https://www.woodmac.com/, last access 27 August 2026). These sources provide estimates for the marketed O&G on asset and field level. Our airborne observations covered areas accounting for approximately 15 % of Oman's marketed O&G production. We aggregated these data to cover areas/facilities/industrial clusters encompassed by the MTG-Oman campaign to obtain an estimate for the CH_4 loss rates. Lastly, we use the total O&G production statistic for Oman of the Ministry of Energy and Mining (MEM, 2023) to compare loss rates of our measurements to national-level estimates from other studies and inventories.

3 Results

In this section, we present the results from a ground-based well survey (Sect. 3.1) and top-down CH_4 mass flux estimates based on the *HELiPOD* measurement for the three regions in northern and southern Oman (Sect. 3.2). Furthermore, we use mobile ground-based measurements, airborne and satellite measurements to disentangle emissions from a cluster of O&G facilities (Sect. 3.3).

3.1 Ground-based well survey

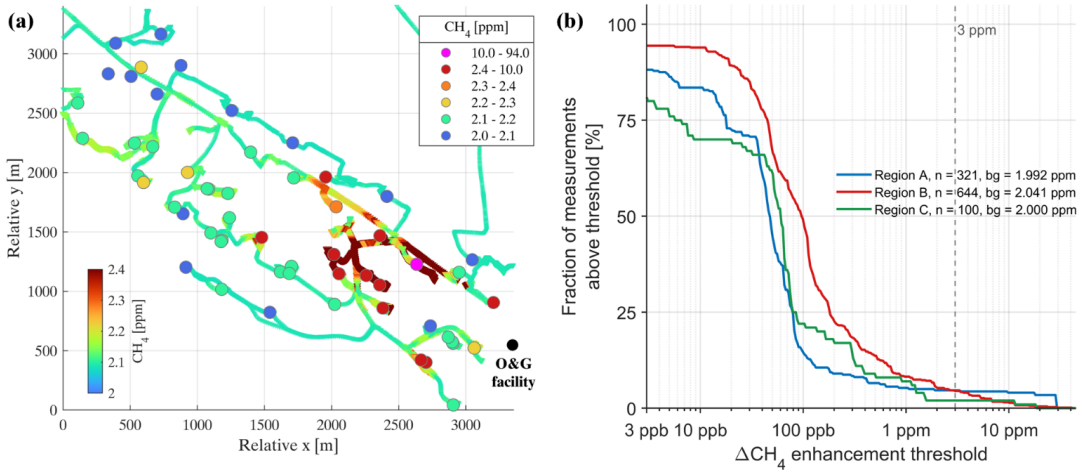
Comprehensive well surveys were conducted on multiple days during MTG-Oman, performing CH_4 measurements in the immediate vicinity (within several metres) of wells and pipelines. In Regions A and B, 30 to 90 % of the active wells were surveyed, while coverage in Region C ranged from 6 to 50 %. Regions A and B consisted exclusively of sweet facilities, whereas Region C comprised only sour facilities.

Figure 4a illustrates a representative example of mobile ground-based CH_4 measurements conducted around oil and gas infrastructure. The measurement pattern reflects targeted sampling of individual well pads (indicated by coloured circles), combined with repeated transects along connecting pipelines and across the surrounding area. Elevated CH_4 concentrations are observed in the central part of the domain, where multiple high enhancements (dark red and pink colours) cluster spatially along the measurement tracks. While the nearby O&G facility could potentially contribute to the observed cluster through transported emissions, the plume structure and measurement geometry indicate a more localised origin. Under weak and locally variable southeasterly wind conditions on this day, long-range transport from the facility is limited, and the spatial alignment of enhancements with well locations points towards emissions from a number of individual wells as the dominant source.

This local-scale behaviour is reflected in the statistical analysis shown in Fig. 4b, which presents cumulative distribution functions (CDFs) of CH_4 enhancements measured several metres downwind of the monitored wells in the three investigated regions (i.e. the distribution of the coloured dots in Fig. 4a). Subdivision into CDFs for only single asset wells is shown in Fig. S3. The atmospheric CH_4 background is determined as the 5^{th} percentile of all measurements within each respective region. A CH_4 enhancement threshold of 3 ppb above the regional background is used to define detectable enhancements. The resulting distributions reveal clear differences in both enhancement magnitude and detection frequency.

https://doi.org/10.5194/egusphere-2026-5294
Preprint. Discussion started: 16 November 2026
© Author(s) 2026. CC BY 4.0 License.

345 Differences in detection frequency are already apparent at the lower end of the distributions: deviations from 100 % at the starting points correspond to the fraction of wells with enhancements below the 3 ppb threshold. Region B shows detectable CH_4 enhancements at most of the wells, whereas the starting points of Regions A and C indicate that approximately 10 % and 20 % of the wells, respectively, show no detectable enhancement above the regional background.



350 **Figure 4.** Ground-based CH_4 measurement survey around O&G well and pipeline infrastructure. (a) Survey section from 21 November, including 56 investigated wells along approximately 40 km of driven survey tracks. The driven path is colour-coded by CH_4 concentration, while well positions are indicated by markers coloured according to the maximum observed CH_4 enhancement. (b) Cumulative distribution of CH_4 enhancements measured several metres downwind of *n* wells in Regions A, B, and C. The atmospheric CH_4 background (bg) is determined as the 5th percentile of all measurements in the respective
355 region. A value of 3 ppb above the regional background is used to define detectable CH_4 enhancements and marks the lower limit of the x-axis. This value corresponds to a 3σ threshold, with σ representing the LI-COR 7810 precision of ~1 ppb at 1 Hz. Deviations from 100 % in the starting points of the cumulative distribution functions (CDFs) correspond to the fraction of wells with enhancements below the 3 ppb threshold.

360 At low enhancement levels (<3 ppm), Region B (sweet gas fields) exhibits a higher fraction of measurements than Regions A and C, indicating a dominance of small but widespread emissions. This behaviour is consistent with the presence of more aged infrastructure, which is typically associated with diffuse and persistent leakage sources. The crossover of the CDF curves at approximately 3 ppm highlights a shift in the relative contribution of larger enhancement events. Above this threshold, Region A shows a comparatively higher fraction of large enhancements than Region B, whereas Region C remains consistently below
365 Region B across the full range of enhancement levels, indicating generally lower overall enhancement magnitudes. This is consistent with Region C representing sour gas infrastructure, where stricter safety requirements due to H_2S handling typically necessitate more rigorous leak prevention. Together, these patterns support the interpretation that Region B is characterised by widespread low-level leakage, Region A by a mixture of non-emitting and strongly emitting wells, and Region C by comparatively tighter infrastructure.

370 **3.2 Methane emission estimates of individual assets**

The overall top-down CH_4 emissions of selected O&G assets were estimated using the helicopter-borne mass balance approach (an example flight pattern is shown in Fig. S4). The resulting top-down CH_4 mass flux estimates for Targets 1 to 6 and corresponding operator-provided bottom-up estimates are presented in Fig. 5. Target-specific mean estimates are summarised in Table 2, while the individual mass flux estimates and detailed meteorological information are listed in Table S5. Further

https://doi.org/10.5194/egusphere-2026-5294
Preprint. Discussion started: 16 November 2026
© Author(s) 2026. CC BY 4.0 License.

details on the calculation method are provided in Sect. 2.3 and Förster et al. (2025). Bottom-up estimates were provided by the operator for all investigated targets. According to the operator, more than 90 % of the reported emissions are based on source-specific measurements or engineering calculations. Fugitive emissions are quantified from measurements of individual leaks, and facility-specific emission factors are applied where measurements are available.

In Region A, emissions originating from Target 1 could be separated into an oil- and a gas-producing facility during one flight, each contributing approximately 50 % to the total emission rate of 200 to 300 kg h^{-1}. For the remaining flights and targets, separation of co-located oil and gas facilities was not possible because a minimum safety flight distance of 1 km had to be maintained. At this distance, plume mixing and dilution had already occurred. Emission rates for Target 2 were generally lower (~65 kg h^{-1}) than for Target 1 but remained relatively consistent across the three flights. However, uncertainties for Target 2 reached up to 100 % on 15 and 17 November 2023 due to very small CH_4 enhancements at the 1 km flight distance (mean enhancement: 4 ppb), close to the Picarro precision of ~1 ppb. A lower uncertainty of 60 % was obtained on 18 November 2023, when larger CH_4 enhancements were observed (mean: 15 ppb). Similar effects contributed to the comparatively large uncertainty ranges for Target 1. At first glance, the bottom-up estimates might suggest that the values for Targets 1 and 2 were interchanged. However, checks with the operator confirmed that the target assignments are correct. The operator-provided bottom-up estimates therefore underestimate emissions for Target 1 and overestimate emissions for Target 2 relative to the top-down estimates, while remaining within the same order of magnitude.

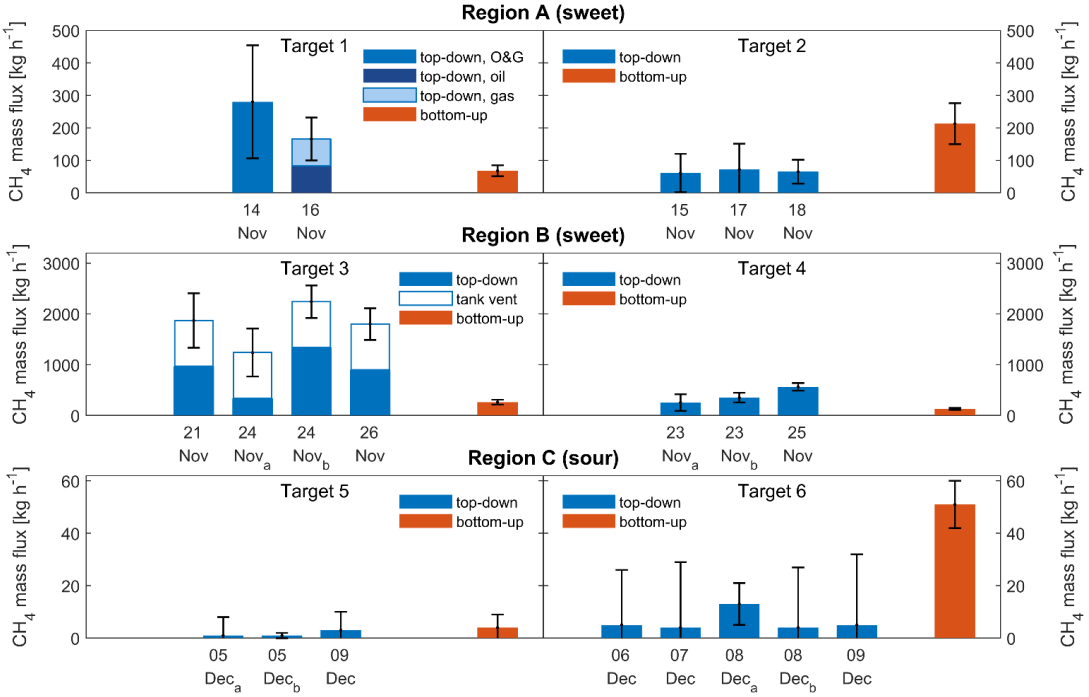


Figure 5. Top-down and bottom-up CH_4 mass flux estimates during MTG-Oman for the three measurement regions: Regions A and B containing sweet assets and Region C containing sour assets, with two targeted O&G assets in each region. The top-down estimates are based on 32 mass balance experiments conducted during 20 flights on 15 measurement days; the subscripted "a" and "b" indicate the first and second flight conducted on the respective day. Error bars represent 1σ uncertainties. Note that each region uses a different y-axis range. Emission rates and detailed meteorological information are provided in Table S5. Bottom-up estimates correspond to the timing of the top-down measurements.

https://doi.org/10.5194/egusphere-2026-5294
Preprint. Discussion started: 16 November 2026
© Author(s) 2026. CC BY 4.0 License.

Assets in Region B covered the widest regional range of emission rates (250 to 2200 kg h^{-1}). This broad range primarily reflects the structural difference between the two targets: Target 3 comprises a cluster of seven facilities, whereas Target 4 is an isolated facility. Within each target, the variability between flights was considerably smaller than the range across the region suggests. Mobile ground-based measurements identified maintenance-related tank venting as a major single source at Target 3. Its estimated flux of approximately 1000 kg h^{-1} accounted for around 50 % of the total measured at this target (light blue bars in Fig. 5; see Sect. 3.3). Top-down estimates for Target 4 ranged between 250 and 560 kg h^{-1}. Compared with these top-down results, the operator-provided bottom-up estimates were lower for both targets in Region B.

If the short-term tank venting event at Target 3 is excluded from the top-down estimates (note that these emissions are also not represented in the bottom-up estimates), only the measurement on 24 November 2023 (morning flight "a") agrees reasonably well with the operator-reported data. However, this flight was conducted under unfavourable wind conditions in a complex topographical landscape. The wind was highly variable and showed pronounced directional changes with height, while the PBL was still developing during the morning hours. Complex flow over the terrain may therefore have diverted part of the plume away from the sampling wall, such that the plume may not have been fully captured. Although the mass balance method and its uncertainty calculation were applied following the standard procedure, this potential sampling limitation is not explicitly represented in the method-derived uncertainty. The corresponding top-down estimate is therefore likely biased low. Consequently, the bottom-up estimates for Region B should be reassessed, taking into account the complete infrastructure as well as intermittent short-term emission events.

Table 2. Comparison of mean top-down CH_4 emission estimates derived from the *HELiPOD* mass balance measurements and corresponding operator-provided bottom-up estimates for the six investigated targets. Mean top-down emissions were calculated from the flight-specific estimates for each target (Table S5). The associated target-specific uncertainties represent the root-mean-square (RMS) of the individual flight uncertainties. Total emissions were calculated as the sums of the six target means. Their uncertainties were conservatively calculated as the linear sums of the target-specific uncertainties. The top-down estimate for B1 includes the maintenance-related tank-venting event observed during the campaign. Mean top-down estimates for C1 and C2 did not exceed the conservative empirical quantification threshold of approximately 16 kg h^{-1}.

Target	Facility type	Flights	Top-down		Bottom-up	
			Mean flux [kg h^{-1}]	uncertainty [kg h^{-1}]	Flux [kg h^{-1}]	uncertainty [kg h^{-1}]
A1	Sweet O&G	2	223	132	68	17
A2	Sweet O&G	3	66	61	213	63
B1	Sweet O&G cluster	4	1788	422	261	48
B2	Sweet O&G	3	389	119	130	19
C1	Sour O&G	3	2	6	4	5
C2	Sour O&G	5	7	22	51	9
Total		20	2474	762	727	162

Finally, Region C comprised only sour facilities, whereas Regions A and B consisted exclusively of sweet facilities, with Targets 5 and 6 exhibiting consistently low CH_4 emissions compared with the facilities in the other two regions. This is illustrated by a measurement example in the Supplement (Figs. S5 and S6), showing downwind CH_4 concentrations close to the background level of ~2 ppm. The mean top-down estimates for both targets (Table 2) did not exceed the conservative empirical quantification threshold of approximately 16 kg h^{-1} (Sect. S2). Bottom-up estimates agreed with the top-down estimate for Target 5 but overestimated emissions for Target 6. Together with the findings in Sect. 3.1 and previous evidence from sour production regions (Lavoie et al., 2022), the consistently low top-down emissions at both targets indicate that the technical and operational controls required for the safe handling of H_2S, including tightly sealed infrastructure, also effectively

https://doi.org/10.5194/egusphere-2026-5294
Preprint. Discussion started: 16 November 2026
© Author(s) 2026. CC BY 4.0 License.

limit CH_4 emissions. This demonstrates the technical feasibility of applying comparable controls through stringent CH_4 regulations to substantially reduce emissions from O&G facilities.

3.3 Multi-scale integration of CH_4 emissions in a complex landscape

During well surveys between 21 and 24 November 2023, mobile ground-based measurements in Region B identified a potential super-emitting source continuously releasing CH_4 and producing enhancements of up to 94 ppm. Satellite measurements detected the same emission event on 22 November 2023 and estimated an emission rate of approximately 1000 kg h^{-1}. This short-term release was associated with maintenance work at the facility. Helicopter-borne mass balance measurements performed on 24 November estimated total CH_4 emissions of approximately 2200 kg h^{-1} for the entire O&G cluster. The combined results from the three complementary measurement systems are shown in Fig. 6 and allow clustered emissions to be disentangled across spatial scales.

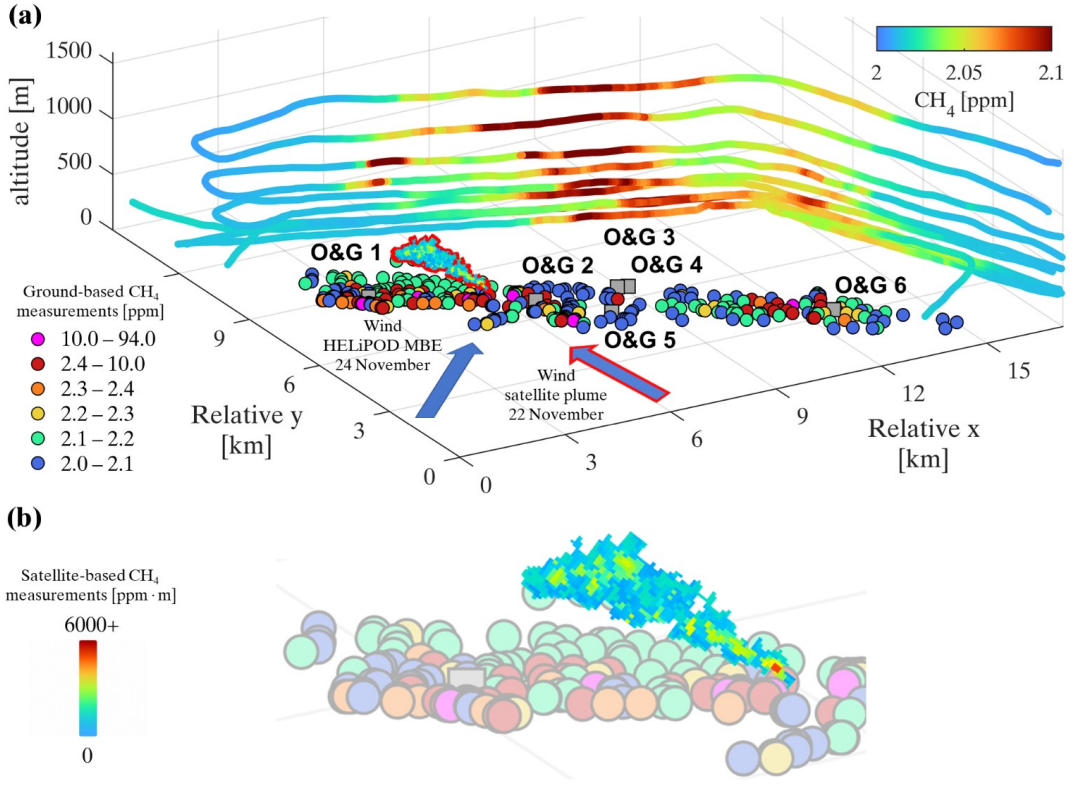


Figure 6. (a) Composite of ground-based measurements (coloured dots showing CH_4 enhancements near wells as measured by the mobile ground-based survey), satellite observations on 22 November 2023 (red-edged plume), and helicopter-borne measurements on 24 November 2023 afternoon (coloured flight tracks); arrows indicate the corresponding wind directions. Grey squares mark six O&G production stations. Ground-based measurements were conducted exclusively as part of the well survey; no additional ground transects were performed beneath the helicopter flight paths because suitable road access was limited across the broad sampling wall and the plume was already sufficiently mixed several kilometres downwind of the sources. (b) Enlarged view of the satellite plume from 22 November 2023. The satellite-derived emission estimate was ~1000 kg h^{-1}, whereas the helicopter-derived estimate for the entire O&G cluster was ~2200 kg h^{-1}.

https://doi.org/10.5194/egusphere-2026-5294
Preprint. Discussion started: 16 November 2026
© Author(s) 2026. CC BY 4.0 License.

Ground-based measurements revealed leakages from wells distributed across the entire cluster, ranging from small to moderate CH_4 enhancements (blue and green dots) to larger enhancements between 2.4 and 94 ppm (yellow and dark red dots), as discussed in Sect. 3.1. The helicopter-borne measurements captured the cumulative contribution of these spatially distributed sources as a broad CH_4 enhancement along the sampling wall (green colours in Fig. 6). Within this broad enhancement, three distinct maxima with substantially higher CH_4 concentrations are visible (red colours). The broad central plume reflects the combined contributions of the maintenance-related venting event, which remained active on 24 November 2023 according to the ground-based measurements, and emissions from O&G facilities 2 to 5. The two smaller maxima flanking this plume are probably associated with emissions from O&G facilities 1 and 6, respectively. Because the wind direction changed between 22 and 24 November 2023, the satellite-observed and airborne plumes do not visually align in the composite.

The combined observations demonstrate that helicopter-borne measurements can quantify not only large point-source emissions but also the cumulative contribution of smaller and spatially distributed emissions originating from production stations and leaking infrastructure. These smaller but persistent sources were not detected by satellite observations because of the comparatively high detection limit, but together accounted for more than 50 % of the total cluster emissions. This is consistent with previous findings highlighting the importance of distributed background emissions (e.g. Williams et al., 2025). At the same time, non-routine emission events associated with maintenance work, abnormal tank venting, or equipment malfunctions can generate extreme short-term releases detectable by satellite observations and may dominate total CH_4 emissions over short periods (Alvarez et al., 2018; Conrad et al., 2023; Naus et al., 2023). Such super-emitting events may not be adequately represented in inventories or operator-reported emissions (Schuit et al., 2023; Chan et al., 2024), which is also reflected in the discrepancies between bottom-up and top-down estimates observed in this study (Sect. 3.2).

4 Discussion

This discussion places the measured emissions in the context of available inventories for Oman and observation-based estimates of other regions and assesses the insights gained by combining measurements across spatial scales. We first examine derived loss rates and discuss limitations of broader extrapolation. We then discuss how ground-based, helicopter-borne, and satellite observations can complement each other in detecting, attributing, and quantifying CH_4 emissions from O&G facilities.

4.1 Comparison and discussion of loss rates

To compare the CH_4 emissions obtained during MTG-Oman with available O&G inventories and previous studies worldwide, we use marketed O&G-production-normalised CH_4 loss rates (Sect. 2.5). The six investigated assets had a combined loss rate of 0.20 ± 0.07 %. For comparison with gas-normalised literature values, the corresponding gas-production-normalised loss rate is 0.58 ± 0.26 %. Both rates were calculated from the total emission estimate of 2474 ± 762 kg h^{-1} (Table 2) and asset-specific marketed production estimates from Rystad and Wood Mackenzie (Sect. 2.5).

The O&G-production-normalised loss rate of 0.20 ± 0.07 % is close to the GFEI inventory estimate of 0.28 % and substantially lower than the other investigated inventories for Oman. However, it is approximately seven times the operator-provided O&G-production-normalised estimate of 0.03 % for all its assets in 2023 (Fig. 7a). Excluding the maintenance-related super-emitting event of approximately 1000 kg h^{-1} results in an alternative loss-rate estimate of 0.12 ± 0.07 %, which remains approximately four times the operator-derived value. The comparison therefore illustrates the strong influence of non-routine high-emission events on short-term top-down estimates, while also indicating that the maintenance-related event alone does not fully explain the difference from the operator estimate. Differences in spatial coverage, temporal representativeness, and estimation methods may additionally contribute to this discrepancy.

The CH_4 loss rates derived for the investigated Omani assets were also generally lower than the loss rates of approximately 0.3 to 3.2 % reported for other O&G regions and study domains in the United States, Canada, and Turkmenistan (Fig. 7b).

https://doi.org/10.5194/egusphere-2026-5294
Preprint. Discussion started: 16 November 2026
© Author(s) 2026. CC BY 4.0 License.

This suggests that, despite the occurrence of a super-emitting event during the campaign, CH_4 emissions from the investigated Omani facilities are relatively moderate compared with those reported for many other major O&G production regions. Possible explanations include effective maintenance practices, comparatively modern infrastructure, and stricter operational and safety requirements, particularly at sour production facilities.

The gas-production-normalised loss rate derived in this study, 0.58 ± 0.26 %, is higher than the corresponding operator-derived value of 0.11 % but substantially lower than the TROPOMI-based estimates reported for Oman by Chen et al. (2023), which range from 4.5 to 13.4 % (Fig. S7 and Table S10). Gasim et al. (2024) considered these comparatively high values to be outliers. The disagreement between estimates derived from the same TROPOMI dataset underscores the need for coordinated ground-based, airborne, and satellite observations to constrain CH_4 emissions, evaluate satellite retrievals, and reduce uncertainties in inventories and satellite-derived emission products.

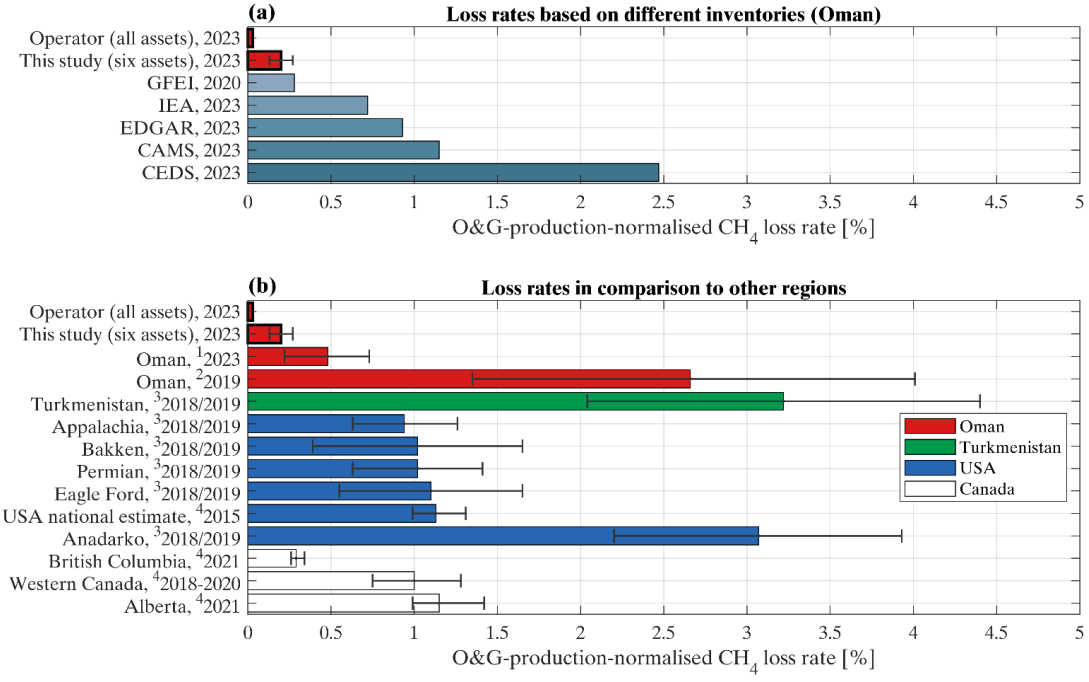


Figure 7. O&G-production-normalised CH_4 loss rates from this study compared with (a) the operator-provided estimate and estimates derived from different emission inventories for Oman and (b) estimates reported for other onshore O&G-producing regions in Oman, the United States, Canada, and Turkmenistan. Inventory-based loss rates in panel (a) were calculated from the respective CH_4 emission estimates and year-matched O&G production statistics from MEM (Table S8). Loss rates in panel (b) were either taken directly from the respective studies or converted to the oil-equivalent mass basis used in this study from reported CH_4 intensities, energy-based O&G loss rates, or gas-production-normalised loss rates. The error bar for this study accounts for uncertainties in the measured emissions and differences between the production estimates from Rystad Energy and Wood Mackenzie (Sect. 2.5). The normalisation and conversion procedures for this study and the publicly available comparison estimates are described in Supplement Sect. S4, and the corresponding input data and derived loss rates are provided in Tables S6 to S9. [1]Gasim et al., 2024, [2]Chen et al., 2023, [3]Schneising et al., 2020, [4]Conrad et al., 2023

At the same time, the interpretation and broader representativeness of the comparisons presented here are constrained by spatial, temporal, and participation-related limitations. In particular, airborne mass balance measurements provide short-term

https://doi.org/10.5194/egusphere-2026-5294
Preprint. Discussion started: 16 November 2026
© Author(s) 2026. CC BY 4.0 License.

snapshots that can vary with operational conditions, maintenance, and non-routine venting. Although the six investigated targets accounted for approximately 15 % of Oman's marketed O&G production, this sample is insufficient for robust national upscaling. Furthermore, opt-in study designs may favour participation by operators with comparatively lower-emitting infrastructure, and workers may be more attentive to operational procedures and maintenance activities when measurement teams are on site or expected to arrive. The magnitude of these potential biases is difficult to quantify. Consequently, the measured loss rates characterise the investigated assets but should not be interpreted as nationally representative estimates for Oman.

4.2 Complementarity of multi-scale methane observations

During MTG-Oman, mobile ground-based surveys detected CH_4 enhancements within several metres of individual wells, with maxima ranging from 3 to 94 ppm. Comparable mobile surveys were conducted by Korbeń et al. (2022) in Romania, where more than 1000 O&G sites were qualitatively screened and approximately 65 % of the sites showed detectable CH_4 emissions. Follow-up measurements by Kuhlmann et al. (2025) revealed significantly fewer detectable emissions than predicted from the earlier survey in Romania, suggesting a CH_4 emission reduction of approximately 20 to 60 % between 2019 and 2021, likely due to mitigation measures and infrastructure improvements implemented after the initial survey campaign. These findings demonstrate that mobile ground-based measurements with precise instrumentation can help raise operator awareness of previously unknown leakages that may not be identified during routine leak detection and repair (LDAR) activities using Optical Gas Imaging (OGI).

The operator conducts OGI surveys at its assets in Oman and reports detectable leakage at fewer than 5 % of the monitored wells. However, the substantially higher sensitivity of high-precision CH_4 analysers, such as those used in this study, enables the detection of smaller emission sources and thus provides a valuable complement to existing LDAR activities. As a direct outcome of the campaign, the operator implemented additional mobile ground-based CH_4 surveys alongside existing LDAR activities to improve the identification of leaking infrastructure. In addition, such measurements provide valuable qualitative information on the spatial distribution of leaking wells and the general magnitude of CH_4 emissions across different O&G facilities and regions. However, mobile ground-based measurements alone generally do not allow robust quantification of integrated facility-scale emissions because the vertical extent and atmospheric transport of the observed plumes are often insufficiently constrained.

Between 2023 and 2025, only a limited number of CH_4 plumes have been detected and quantified by satellite observations in Oman compared to other major O&G-producing regions. Reported satellite-derived emission rates range from approximately 200 kg h^{-1} to more than 4000 kg h^{-1} (see https://methanedata.unep.org/ and https://data.carbonmapper.org, last access: 27 August 2026). Approximately 75 % of these detected plumes were classified as super-emitters with emission rates exceeding 500 kg h^{-1}. This highlights that current satellite systems are highly effective at locating large emission sources and enabling rapid mitigation actions, but often miss the large number of smaller, diffuse, or spatially distributed emission sources due to their detection thresholds and sensitivity to atmospheric and surface conditions.

Helicopter-borne observations provide an important observational bridge between localised ground-based measurements and large-scale satellite observations. During MTG-Oman, the helicopter-borne system captured emission rates between approximately 60 and 2200 kg h^{-1}, while previous measurements with *HELiPOD* in Poland demonstrated its capability to quantify emissions ranging from approximately 20 kg h^{-1} to more than 5000 kg h^{-1} under suitable conditions (Förster et al., 2025). In contrast to satellite observations, helicopter-borne mass balance measurements can characterise not only isolated super-emitters but also diffuse and spatially distributed emissions across complex facility clusters. Nevertheless, airborne observations remain sensitive to meteorological conditions and, as discussed in Sect. 4.1, provide only short-term snapshots of the emission landscape, possibly under opt-in conditions.

https://doi.org/10.5194/egusphere-2026-5294
Preprint. Discussion started: 16 November 2026
© Author(s) 2026. CC BY 4.0 License.

Together, the combined observations demonstrate that no single observing system is sufficient to comprehensively characterise CH_4 emissions from complex O&G landscapes. Ground-based measurements provide detailed source attribution and leak identification at individual wells, whereas satellites efficiently detect major super-emitting events over broad regions. Helicopter-borne mass balance observations complement both approaches by integrating emissions across entire facility clusters, including diffuse and persistent sources that are often not resolved by satellite observations or represented in inventories. Coordinated ground-based, airborne, and satellite measurements therefore provide a powerful framework for validating inventories, constraining satellite retrievals, and improving CH_4 emission estimates across multiple spatial scales.

5 Summary & conclusion

The Arabian Peninsula is one of the world's major O&G-producing regions, yet CH_4 emissions from the sector remain highly uncertain, with substantial discrepancies between inventories, satellite-based estimates, and national reporting. At the same time, independent observation-based constraints remain scarce. Given Oman's commitments under the Global Methane Pledge and 2050 net-zero target, METHANE-To-Go-Oman addressed this gap through the first airborne GHG campaign on the Arabian Peninsula, using the helicopter-towed *HELiPOD* platform complemented by mobile ground-based measurements. Operating *HELiPOD* as an external sling load with a local helicopter company provided a flexible airborne verification capability suited to regions where conventional research aircraft operations are difficult, while simplifying logistics and flight permissions and avoiding the need for dedicated aircraft certification. Between 14 November and 9 December 2023, 22 O&G-targeted mission flights investigated six assets in three regions of northern and southern Oman, representing approximately 15 % of the country's marketed O&G production.

Airborne measurements quantified emission rates of approximately 60 to 2200 kg h^{-1} for individual sweet facilities and facility clusters processing hydrocarbons with negligible sulfur and CO_2 content. In contrast, all emission estimates for the investigated sour facilities, which handle sulfur- and/or CO_2-rich streams, remained below the empirical *HELiPOD* quantification threshold of approximately 16 kg h^{-1}, indicating very low CH_4 emissions at the time of measurement. Mobile ground-based surveys of wells, pipelines, and other O&G infrastructure detected CH_4 enhancements within several metres of the surveyed components. Maximum enhancements across the investigated assets ranged from 3 to 94 ppm, with the highest value associated with a maintenance-related emission event. A regional comparison of these measurements showed a higher overall prevalence of CH_4 emissions around sweet facilities than around sour facilities, reflected in both a larger number of detected leaks and a higher frequency of small CH_4 enhancements. The surveys also identified a maintenance-related super-emitting event at a sweet facility cluster, which was independently detected and quantified by satellite observations at approximately 1000 kg h^{-1}. Airborne and ground-based measurements thus consistently indicated that CH_4 emissions were higher at sweet facilities than at sour facilities. These findings support previous evidence that the technical and operational controls required for the safe handling of H_2S, including tightly sealed infrastructure, also limit CH_4 emissions. They further demonstrate that comparable controls are technically feasible and could substantially reduce emissions from O&G facilities if required through stringent CH_4 regulations.

Helicopter-borne top-down and operator-provided bottom-up estimates were of the same order of magnitude for individual facilities, whereas the top-down estimate for a complex facility cluster was approximately seven times higher than the corresponding bottom-up estimate, partly because the maintenance-related emission event was not captured by the latter. To compare these emission estimates with inventories and other producing regions, marketed O&G-production-normalised CH_4 loss rates were derived. Total marketed O&G production rather than gas production alone was used as the primary denominator because half of the targeted assets produced oil only. The resulting loss rate was 0.20 ± 0.07 % for the investigated facilities, substantially lower than most inventory-based estimates for Oman, which ranged from 0.3 to 2.5 %, but approximately seven times the operator-provided O&G-production-normalised estimate of 0.03 %. Excluding the maintenance-related event results

https://doi.org/10.5194/egusphere-2026-5294
Preprint. Discussion started: 16 November 2026
© Author(s) 2026. CC BY 4.0 License.

in a loss rate of 0.12 ± 0.07 %, which remains approximately four times the operator estimate. This illustrates the strong influence of non-routine operational events on short-term top-down estimates while indicating that the maintenance-related event alone does not fully account for the difference from the operator estimate. Compared with previous studies from major production regions in the United States, Canada, and Turkmenistan, which reported O&G-production-normalised loss rates of approximately 0.3 to 3.2 %, the investigated Omani assets exhibited generally lower loss rates. For comparison on a gas-production basis, the corresponding loss rate was 0.58 ± 0.26 % with the super-emitting event included, exceeding both the operator-provided gas-production-normalised estimate of 0.11 % and the OGCI target of 0.20 %.

Combining ground-based, airborne, and satellite observations provides complementary perspectives on the emission landscape: ground surveys localise individual sources, satellites identify and quantify the large emission events, and *HELiPOD* validates these observations while quantifying integrated emissions from entire facility clusters, including smaller, spatially dispersed sources below satellite detection limits. Helicopter-borne measurements thus bridge the observational gap between localised ground-based surveys and large-scale satellite observations. The results demonstrate the value of coordinated multi-scale observations for evaluating inventories and satellite products and identifying mitigation opportunities. Specifically, the measurements highlight the need to combine high-sensitivity detection and prompt repair of small leaks with operational measures to prevent or minimise high-emission releases, for example by avoiding or reducing venting during maintenance and other non-routine operations.

As the measurements provide only a first, spatially and temporally limited snapshot covering part of Oman's marketed O&G production, further coordinated observations using such integrated measurement approaches are needed across the Arabian Peninsula and other O&G-producing regions to extend spatial and temporal coverage and support independent monitoring and verification of CH_4 emissions.

Data availability. The methane data with relative coordinates for each investigated target are currently undergoing final quality control and preparation for deposition in the ICOS Carbon Portal. The data will be assigned a DOI, which will be added to the manuscript as soon as it becomes available and before potential final publication. During peer review, the data supporting the analyses can be made available to the editor and reviewers upon request.

This Manuscript contains modified Copernicus Atmosphere Monitoring Service information [2025]. Neither the European Commission nor ECMWF is responsible for any use that may be made of the Copernicus information or data it contains.

Supplement. The supplement related to this article is available separately.

Author contributions. The paper was written and the figures were prepared by EF with contributions from HH and ML. The experimental design and flight planning were performed by HH, EF, FP, NM and AR. *HELiPOD* supervision and data processing were performed by FP, LB, SB, AS and AL. Mobile ground-based measurements were conducted and processed by PJ, JB and JN. BW supported ground-based on-site measurements to retrieve boundary layer height information. All authors contributed to the discussion of the results and the improvement of the manuscript.

Competing interests. The authors declare that they have no conflict of interest.

Acknowledgements. We gratefully acknowledge the support of our local industry partner, whose collaboration was essential for the successful execution of the campaign, including access to facilities and the provision of valuable operational insights. We also thank Yassine Charabi for his support in an early stage of the MTG-Oman project and for facilitating important local contacts that helped paving the way for the conducted field experiment. We thank the helicopter pilots Ivan van Rooyen and Kevin Patten, as well as Al Sharqiya Aviation (ASA), for their professional support and excellent cooperation during the flight

https://doi.org/10.5194/egusphere-2026-5294
Preprint. Discussion started: 16 November 2026
© Author(s) 2026. CC BY 4.0 License.

operations. We further thank Siham Salim Al Hadhrami for her local support and assistance during the METHANE-To-Go-Oman campaign. Finally, we thank Maciej Bartosiewicz for his helpful comments and suggestions, which contributed to improving this manuscript.

AI tools like ChatGPT, Gemini and Ollama were used in light editing of this manuscript and code generation.

Financial support. This research has been funded in the framework of UNEP's International Methane Emissions Observatory (IMEO). Ground-based measurements were additionally supported by AGH University of Kraków within the Excellence Initiative – Research University programme.

References

Albusaidi, J.: Integrating air quality and climate change strategies in Oman, PhD Thesis, University of York, 2019.

Allen, D.: Attributing Atmospheric Methane to Anthropogenic Emission Sources, Acc. Chem. Res., 49, 1344–1350, https://doi.org/10.1021/acs.accounts.6b00081, 2016.

Al-Shidhani, M. A. and Hayyan, M.: Oman's energy transition roadmap to net zero 2050, Energy Nexus, 19, 100493, https://doi.org/10.1016/j.nexus.2025.100493, 2025.

Alvarez, R. A., Zavala-Araiza, D., Lyon, D. R., Allen, D. T., Barkley, Z. R., Brandt, A. R., Davis, K. J., Herndon, S. C., Jacob, D. J., Karion, A., Kort, E. A., Lamb, B. K., Lauvaux, T., Maasakkers, J. D., Marchese, A. J., Omara, M., Pacala, S. W., Peischl, J., Robinson, A. L., Shepson, P. B., Sweeney, C., Townsend-Small, A., Wofsy, S. C., and Hamburg, S. P.: Assessment of methane emissions from the U.S. oil and gas supply chain, Science, 361, 186–188, https://doi.org/10.1126/science.aar7204, 2018.

Ayasse, A. K., Thorpe, A. K., Cusworth, D. H., Kort, E. A., Negron, A. G., Heckler, J., Asner, G., and Duren, R. M.: Methane remote sensing and emission quantification of offshore shallow water oil and gas platforms in the Gulf of Mexico, Environ. Res. Lett., 17, 084039, https://doi.org/10.1088/1748-9326/ac8566, 2022.

Barkley, Z. R., Davis, K. J., Miles, N. L., and Richardson, S. J.: Examining Daily Temporal Characteristics of Oil and Gas Methane Emissions in the Delaware Basin Using Continuous Tower Observations, Journal of Geophysical Research: Atmospheres, 130, e2024JD042050, https://doi.org/10.1029/2024JD042050, 2025.

Bourtsoukidis, E., Germain-Piaulenne, E., Gros, V., Quéhé, P.-Y., Pikridas, M., Byron, J., Williams, J., Gliddon, D., Mohamed, R., Ekaabi, R., Lelieveld, J., Sciare, J., Teixidó, O., and Paris, J.-D.: Attribution of Excess Methane Emissions Over Marine Environments of the Mediterranean and Arabian Peninsula, Journal of Geophysical Research: Atmospheres, 129, e2024JD041621, https://doi.org/10.1029/2024JD041621, 2024.

Brandt, A. R., Heath, G. A., Kort, E. A., O'Sullivan, F., Pétron, G., Jordaan, S. M., Tans, P., Wilcox, J., Gopstein, A. M., Arent, D., Wofsy, S., Brown, N. J., Bradley, R., Stucky, G. D., Eardley, D., and Harriss, R.: Methane Leaks from North American Natural Gas Systems, Science, 343, 733–735, https://doi.org/10.1126/science.1247045, 2014.

Cambaliza, M. O. L., Shepson, P. B., Caulton, D. R., Stirm, B., Samarov, D., Gurney, K. R., Turnbull, J., Davis, K. J., Possolo, A., Karion, A., Sweeney, C., Moser, B., Hendricks, A., Lauvaux, T., Mays, K., Whetstone, J., Huang, J., Razlivanov, I., Miles, N. L., and Richardson, S. J.: Assessment of uncertainties of an aircraft-based mass balance approach for quantifying urban greenhouse gas emissions, Atmos. Chem. Phys., 14, 9029–9050, https://doi.org/10.5194/acp-14-9029-2014, 2014.

Chan, E., Vogel, F., Smyth, S., Barrigar, O., Ishizawa, M., Kim, J., Neish, M., Chan, D., and Worthy, D. E. J.: Hybrid bottom-up and top-down framework resolves discrepancies in Canada's oil and gas methane inventories, Commun Earth Environ, 5, 566, https://doi.org/10.1038/s43247-024-01728-6, 2024.

Charabi, Y.: Digging deeper into cutting methane emissions from the oil and gas industry in the era of volatile prices, Mitig Adapt Strateg Glob Change, 26, 6, https://doi.org/10.1007/s11027-021-09948-3, 2021.

Chen, Z., Jacob, D. J., Gautam, R., Omara, M., Stavins, R. N., Stowe, R. C., Nesser, H., Sulprizio, M. P., Lorente, A., Varon, D. J., Lu, X., Shen, L., Qu, Z., Pendergrass, D. C., and Hancock, S.: Satellite quantification of methane emissions and oil–gas

https://doi.org/10.5194/egusphere-2026-5294
Preprint. Discussion started: 16 November 2026
© Author(s) 2026. CC BY 4.0 License.

methane intensities from individual countries in the Middle East and North Africa: implications for climate action, Atmospheric Chemistry and Physics, 23, 5945–5967, https://doi.org/10.5194/acp-23-5945-2023, 2023.

Conley, S., Faloona, I., Mehrotra, S., Suard, M., Lenschow, D. H., Sweeney, C., Herndon, S., Schwietzke, S., Pétron, G., Pifer, J., Kort, E. A., and Schnell, R.: Application of Gauss's theorem to quantify localized surface emissions from airborne measurements of wind and trace gases, Atmospheric Measurement Techniques, 10, 3345–3358, https://doi.org/10.5194/amt-10-3345-2017, 2017.

Conrad, B. M., Tyner, D. R., Li, H. Z., Xie, D., and Johnson, M. R.: A measurement-based upstream oil and gas methane inventory for Alberta, Canada reveals higher emissions and different sources than official estimates, Commun Earth Environ, 4, 416, https://doi.org/10.1038/s43247-023-01081-0, 2023.

Crosson, E. R.: A cavity ring-down analyzer for measuring atmospheric levels of methane, carbon dioxide, and water vapor, Appl. Phys. B, 92, 403–408, https://doi.org/10.1007/s00340-008-3135-y, 2008.

Dai, C., Wang, Q., Kalogiros, J. A., Lenschow, D. H., Gao, Z., and Zhou, M.: Determining Boundary-Layer Height from Aircraft Measurements, Boundary-Layer Meteorol, 152, 277–302, https://doi.org/10.1007/s10546-014-9929-z, 2014.

Duren, R. M., Thorpe, A. K., Foster, K. T., Rafiq, T., Hopkins, F. M., Yadav, V., Bue, B. D., Thompson, D. R., Conley, S., Colombi, N. K., Frankenberg, C., McCubbin, I. B., Eastwood, M. L., Falk, M., Herner, J. D., Croes, B. E., Green, R. O., and Miller, C. E.: California's methane super-emitters, Nature, 575, 180–184, https://doi.org/10.1038/s41586-019-1720-3, 2019.

EIA: U.S. Energy Information Administration (EIA), https://www.eia.gov/international/data/world (last access: 15 April 2025), 2025.

Esparza, Á. E., Rowan, G., Newhook, A., Deglint, H. J., Garrison, B., Orth-Lashley, B., Girard, M., and Shaw, W.: Analysis of a tiered top-down approach using satellite and aircraft platforms to monitor oil and gas facilities in the Permian basin, Renewable and Sustainable Energy Reviews, 178, 113265, https://doi.org/10.1016/j.rser.2023.113265, 2023.

Förster, E., Huntrieser, H., Lichtenstern, M., Pätzold, F., Bretschneider, L., Schlerf, A., Bollmann, S., Lampert, A., Nęcki, J., Jagoda, P., Swolkień, J., Pasternak, D., Field, R. A., and Roiger, A.: A helicopter-based mass balance approach for quantifying methane emissions from industrial activities, applied for coal mine ventilation shafts in Poland, Atmos. Meas. Tech., 18, 7153–7176, https://doi.org/10.5194/amt-18-7153-2025, 2025.

Forster, P., Storelvmo, T., Armour, K., Collins, W., Dufresne, J.-L., Frame, D., Lunt, D. J., Mauritsen, T., Palmer, M. D., Watanabe, M., Wild, M., and Zhang, H.: The Earth's Energy Budget, Climate Feedbacks, and Climate Sensitivity. In Climate Change 2021: The Physical Science Basis. Contribution of Working Group I to the Sixth Assessment Report of the Intergovernmental Panel on Climate Change, 1st ed., Cambridge University Press, https://doi.org/10.1017/9781009157896, 2021.

Frankenberg, C., Thorpe, A. K., Thompson, D. R., Hulley, G., Kort, E. A., Vance, N., Borchardt, J., Krings, T., Gerilowski, K., Sweeney, C., Conley, S., Bue, B. D., Aubrey, A. D., Hook, S., and Green, R. O.: Airborne methane remote measurements reveal heavy-tail flux distribution in Four Corners region, Proceedings of the National Academy of Sciences, 113, 9734–9739, https://doi.org/10.1073/pnas.1605617113, 2016.

Gasim, A., Matar, W., Muhsen, A., Anand, S., and Guery, J.: Using Satellite Technology to Measure Methane Emissions in Arabian Gulf Countries, King Abdullah Petroleum Studies and Research Center, https://doi.org/10.30573/KS--2024-DP38, 2024.

Germain-Piaulenne, E., Paris, J.-D., Gros, V., Quéhé, P.-Y., Pikridas, M., Baisnée, D., Berchet, A., Sciare, J., and Bourtsoukidis, E.: Middle East oil and gas methane emissions signature captured at a remote site using light hydrocarbon tracers, Atmospheric Environment: X, 22, 100253, https://doi.org/10.1016/j.aeaoa.2024.100253, 2024.

Gorroño, J., Varon, D. J., Irakulis-Loitxate, I., and Guanter, L.: Understanding the potential of Sentinel-2 for monitoring methane point emissions, Atmospheric Measurement Techniques, 16, 89–107, https://doi.org/10.5194/amt-16-89-2023, 2023.

Huang, Q., Li, F., Yan, Y., Bai, S., Zhou, C., Zhou, W., and Zhang, Y.: Four-Year Assessment of Methane Point Source Emissions in the Middle East and North Africa Using Multiple Hyperspectral Satellite Observations, JGR Atmospheres, 131, e2025JD044051, https://doi.org/10.1029/2025JD044051, 2026.

IEA: Global Methane Tracker 2024, Paris, https://www.iea.org/reports/global-methane-tracker-2024 (last access: 15 April 2025), 2024.

https://doi.org/10.5194/egusphere-2026-5294
Preprint. Discussion started: 16 November 2026
© Author(s) 2026. CC BY 4.0 License.

IMEO: International Methane Emissions Observatory (IMEO), https://www.unep.org/topics/energy/methane/international-methane-emissions-observatory, last access: 27 August 2026, 2026.

Irakulis-Loitxate, I., Guanter, L., Liu, Y.-N., Varon, D. J., Maasakkers, J. D., Zhang, Y., Chulakadabba, A., Wofsy, S. C., Thorpe, A. K., Duren, R. M., Frankenberg, C., Lyon, D. R., Hmiel, B., Cusworth, D. H., Zhang, Y., Segl, K., Gorroño, J., Sánchez-García, E., Sulprizio, M. P., Cao, K., Zhu, H., Liang, J., Li, X., Aben, I., and Jacob, D. J.: Satellite-based survey of extreme methane emissions in the Permian basin, Science Advances, 7, eabf4507, https://doi.org/10.1126/sciadv.abf4507, 2021.

Jacob, D. J., Turner, A. J., Maasakkers, J. D., Sheng, J., Sun, K., Liu, X., Chance, K., Aben, I., McKeever, J., and Frankenberg, C.: Satellite observations of atmospheric methane and their value for quantifying methane emissions, Atmospheric Chemistry and Physics, 16, 14371–14396, https://doi.org/10.5194/acp-16-14371-2016, 2016.

Jagoda, P., Nęcki, J., Bartyzel, J., and Swolkień, J.: Mobile measurements of coal mine ventilation shafts in USCB, Poland., 11832, https://doi.org/10.5194/egusphere-egu24-11832, 2024.

Johnson, M. R., Tyner, D. R., and Conrad, B. M.: Origins of Oil and Gas Sector Methane Emissions: On-Site Investigations of Aerial Measured Sources, Environ. Sci. Technol., 57, 2484–2494, https://doi.org/10.1021/acs.est.2c07318, 2023.

Kirschke, S., Bousquet, P., Ciais, P., Saunois, M., Canadell, J. G., Dlugokencky, E. J., Bergamaschi, P., Bergmann, D., Blake, D. R., Bruhwiler, L., Cameron-Smith, P., Castaldi, S., Chevallier, F., Feng, L., Fraser, A., Heimann, M., Hodson, E. L., Houweling, S., Josse, B., Fraser, P. J., Krummel, P. B., Lamarque, J.-F., Langenfelds, R. L., Le Quéré, C., Naik, V., O'Doherty, S., Palmer, P. I., Pison, I., Plummer, D., Poulter, B., Prinn, R. G., Rigby, M., Ringeval, B., Santini, M., Schmidt, M., Shindell, D. T., Simpson, I. J., Spahni, R., Steele, L. P., Strode, S. A., Sudo, K., Szopa, S., van der Werf, G. R., Voulgarakis, A., van Weele, M., Weiss, R. F., Williams, J. E., and Zeng, G.: Three decades of global methane sources and sinks, Nature Geosci, 6, 813–823, https://doi.org/10.1038/ngeo1955, 2013.

Klausner, T., Mertens, M., Huntrieser, H., Galkowski, M., Kuhlmann, G., Baumann, R., Fiehn, A., Jöckel, P., Pühl, M., and Roiger, A.: Urban greenhouse gas emissions from the Berlin area: A case study using airborne CO2 and CH4 in situ observations in summer 2018, Elementa: Science of the Anthropocene, 8, 15, https://doi.org/10.1525/elementa.411, 2020.

Korbeń, P., Jagoda, P., Maazallahi, H., Kammerer, J., Nęcki, J. M., Wietzel, J. B., Bartyzel, J., Radovici, A., Zavala-Araiza, D., Röckmann, T., and Schmidt, M.: Quantification of methane emission rate from oil and gas wells in Romania using ground-based measurement techniques, Elementa: Science of the Anthropocene, 10, 00070, https://doi.org/10.1525/elementa.2022.00070, 2022.

Kuhlmann, G., Stavropoulou, F., Schwietzke, S., Zavala-Araiza, D., Thorpe, A., Hueni, A., Emmenegger, L., Calcan, A., Röckmann, T., and Brunner, D.: Evidence of successful methane mitigation in one of Europe's most important oil production region, Atmospheric Chemistry and Physics, 25, 5371–5385, https://doi.org/10.5194/acp-25-5371-2025, 2025.

Lavoie, M., Baillie, J., Bourlon, E., O'Connell, E., MacKay, K., Boelens, I., and Risk, D.: Sweet and sour: A quantitative analysis of methane emissions in contrasting Alberta, Canada, heavy oil developments, Science of The Total Environment, 807, 150836, https://doi.org/10.1016/j.scitotenv.2021.150836, 2022.

Liu, M., van der A, R., van Weele, M., Bryan, L., Eskes, H., Veefkind, P., Liu, Y., Lin, X., de Laat, J., and Ding, J.: Current potential of CH_4 emission estimates using TROPOMI in the Middle East, Atmospheric Measurement Techniques, 17, 5261–5277, https://doi.org/10.5194/amt-17-5261-2024, 2024.

McDermitt, D., Burba, G., Xu, L., Anderson, T., Komissarov, A., Riensche, B., Schedlbauer, J., Starr, G., Zona, D., Oechel, W., Oberbauer, S., and Hastings, S.: A new low-power, open-path instrument for measuring methane flux by eddy covariance, Appl. Phys. B, 102, 391–405, https://doi.org/10.1007/s00340-010-4307-0, 2011.

McLinden, C. A., Griffin, D., Davis, Z., Hempel, C., Smith, J., Sioris, C., Nassar, R., Moeini, O., Legault-Ouellet, E., and Malo, A.: An Independent Evaluation of GHGSat Methane Emissions: Performance Assessment, Journal of Geophysical Research: Atmospheres, 129, e2023JD039906, https://doi.org/10.1029/2023JD039906, 2024.

MEM: Ministry of Energy and Minerals of Oman (MEM) Annual Report 2023, https://www.scribd.com/document/823696186/MEM-Annual-Report-2023 (last access: 29 September 2025), 2023.

Natural Gas.Org: Processing Natural Gas, https://naturalgas.org/naturalgas/processing-ng/ (last access: 18 December 2025), 2025.

https://doi.org/10.5194/egusphere-2026-5294
Preprint. Discussion started: 16 November 2026
© Author(s) 2026. CC BY 4.0 License.

Naus, S., Maasakkers, J. D., Gautam, R., Omara, M., Stikker, R., Veenstra, A. K., Nathan, B., Irakulis-Loitxate, I., Guanter, L., Pandey, S., Girard, M., Lorente, A., Borsdorff, T., and Aben, I.: Assessing the Relative Importance of Satellite-Detected Methane Superemitters in Quantifying Total Emissions for Oil and Gas Production Areas in Algeria, Environ. Sci. Technol., 57, 19545–19556, https://doi.org/10.1021/acs.est.3c04746, 2023.

Nisbet, E. and Weiss, R.: Top-Down Versus Bottom-Up, Science, 328, 1241–1243, https://doi.org/10.1126/science.1189936, 2010.

O'Callaghan, J.: Tracking methane super-emitters from space, Nature, https://doi.org/10.1038/d41586-024-03594-w, 2024.

OGCI: OGCI Progress Report 2025, https://www.ogci.com/wp-content/uploads/2025/10/251017_OGCI_ProgressReport2025_V21.2.pdf, 2025.

Paris, J.-D., Riandet, A., Bourtsoukidis, E., Delmotte, M., Berchet, A., Williams, J., Ernle, L., Tadic, I., Harder, H., and Lelieveld, J.: Shipborne measurements of methane and carbon dioxide in the Middle East and Mediterranean areas and the contribution from oil and gas emissions, Atmospheric Chemistry and Physics, 21, 12443–12462, https://doi.org/10.5194/acp-21-12443-2021, 2021.

Pätzold, F., Bretschneider, L., Nowak, S., Brandt, B., Schlerf, A., Asmussen, M. O., Bollmann, S., Bärfuss, K., Harm-Altstädter, B., Hecker, P., Wehner, B., van der Wall, B. G., Sachs, T., Huntrieser, H., Roiger, A., and Lampert, A.: HELiPOD—Revolution and evolution of a helicopter-borne measurement system for multidisciplinary research in demanding environments, Elementa: Science of the Anthropocene, 11, 00031, https://doi.org/10.1525/elementa.2023.00031, 2023.

Petrescu, A. M. R., Peters, G. P., Engelen, R., Houweling, S., Brunner, D., Tsuruta, A., Matthews, B., Patra, P. K., Belikov, D., Thompson, R. L., Höglund-Isaksson, L., Zhang, W., Segers, A. J., Etiope, G., Ciotoli, G., Peylin, P., Chevallier, F., Aalto, T., Andrew, R. M., Bastviken, D., Berchet, A., Broquet, G., Conchedda, G., Dellaert, S. N. C., Denier van der Gon, H., Gütschow, J., Haussaire, J.-M., Lauerwald, R., Markkanen, T., van Peet, J. C. A., Pison, I., Regnier, P., Solum, E., Scholze, M., Tenkanen, M., Tubiello, F. N., van der Werf, G. R., and Worden, J. R.: Comparison of observation- and inventory-based methane emissions for eight large global emitters, Earth System Science Data, 16, 4325–4350, https://doi.org/10.5194/essd-16-4325-2024, 2024.

Pühl, M., Roiger, A., Fiehn, A., Gorchov Negron, A. M., Kort, E. A., Schwietzke, S., Pisso, I., Foulds, A., Lee, J., France, J. L., Jones, A. E., Lowry, D., Fisher, R. E., Huang, L., Shaw, J., Bateson, P., Andrews, S., Young, S., Dominutti, P., Lachlan-Cope, T., Weiss, A., and Allen, G.: Aircraft-based mass balance estimate of methane emissions from offshore gas facilities in the southern North Sea, Atmospheric Chemistry and Physics, 24, 1005–1024, https://doi.org/10.5194/acp-24-1005-2024, 2024.

Reid, J. S., Piketh, S. J., Walker, A. L., Burger, R. P., Ross, K. E., Westphal, D. L., Bruintjes, R. T., Holben, B. N., Hsu, C., Jensen, T. L., Kahn, R. A., Kuciauskas, A. P., Al Mandoos, A., Al Mangoosh, A., Miller, S. D., Porter, J. N., Reid, E. A., and Tsay, S.-C.: An overview of UAE2 flight operations: Observations of summertime atmospheric thermodynamic and aerosol profiles of the southern Arabian Gulf, Journal of Geophysical Research: Atmospheres, 113, https://doi.org/10.1029/2007JD009435, 2008.

Roscioli, J. R., Yacovitch, T. I., Floerchinger, C., Mitchell, A. L., Tkacik, D. S., Subramanian, R., Martinez, D. M., Vaughn, T. L., Williams, L., Zimmerle, D., Robinson, A. L., Herndon, S. C., and Marchese, A. J.: Measurements of methane emissions from natural gas gathering facilities and processing plants: measurement methods, Atmospheric Measurement Techniques, 8, 2017–2035, https://doi.org/10.5194/amt-8-2017-2015, 2015.

Saunois, M., Stavert, A. R., Poulter, B., Bousquet, P., Canadell, J. G., Jackson, R. B., Raymond, P. A., Dlugokencky, E. J., Houweling, S., Patra, P. K., Ciais, P., Arora, V. K., Bastviken, D., Bergamaschi, P., Blake, D. R., Brailsford, G., Bruhwiler, L., Carlson, K. M., Carrol, M., Castaldi, S., Chandra, N., Crevoisier, C., Crill, P. M., Covey, K., Curry, C. L., Etiope, G., Frankenberg, C., Gedney, N., Hegglin, M. I., Höglund-Isaksson, L., Hugelius, G., Ishizawa, M., Ito, A., Janssens-Maenhout, G., Jensen, K. M., Joos, F., Kleinen, T., Krummel, P. B., Langenfelds, R. L., Laruelle, G. G., Liu, L., Machida, T., Maksyutov, S., McDonald, K. C., McNorton, J., Miller, P. A., Melton, J. R., Morino, I., Müller, J., Murguia-Flores, F., Naik, V., Niwa, Y., Noce, S., O'Doherty, S., Parker, R. J., Peng, C., Peng, S., Peters, G. P., Prigent, C., Prinn, R., Ramonet, M., Regnier, P., Riley, W. J., Rosentreter, J. A., Segers, A., Simpson, I. J., Shi, H., Smith, S. J., Steele, L. P., Thornton, B. F., Tian, H., Tohjima, Y., Tubiello, F. N., Tsuruta, A., Viovy, N., Voulgarakis, A., Weber, T. S., van Weele, M., van der Werf, G. R., Weiss, R. F., Worthy, D., Wunch, D., Yin, Y., Yoshida, Y., Zhang, W., Zhang, Z., Zhao, Y., Zheng, B., Zhu, Q., Zhu, Q., and Zhuang, Q.: The Global Methane Budget 2000–2017, Earth System Science Data, 12, 1561–1623, https://doi.org/10.5194/essd-12-1561-2020, 2020.

Saunois, M., Martinez, A., Poulter, B., Zhang, Z., Raymond, P. A., Regnier, P., Canadell, J. G., Jackson, R. B., Patra, P. K., Bousquet, P., Ciais, P., Dlugokencky, E. J., Lan, X., Allen, G. H., Bastviken, D., Beerling, D. J., Belikov, D. A., Blake, D. R., Castaldi, S., Crippa, M., Deemer, B. R., Dennison, F., Etiope, G., Gedney, N., Höglund-Isaksson, L., Holgerson, M. A.,

https://doi.org/10.5194/egusphere-2026-5294
Preprint. Discussion started: 16 November 2026
© Author(s) 2026. CC BY 4.0 License.



Hopcroft, P. O., Hugelius, G., Ito, A., Jain, A. K., Janardanan, R., Johnson, M. S., Kleinen, T., Krummel, P. B., Lauerwald, R., Li, T., Liu, X., McDonald, K. C., Melton, J. R., Mühle, J., Müller, J., Murguia-Flores, F., Niwa, Y., Noce, S., Pan, S., Parker, R. J., Peng, C., Ramonet, M., Riley, W. J., Rocher-Ros, G., Rosentreter, J. A., Sasakawa, M., Segers, A., Smith, S. J., Stanley, E. H., Thanwerdas, J., Tian, H., Tsuruta, A., Tubiello, F. N., Weber, T. S., van der Werf, G. R., Worthy, D. E. J., Xi, Y., Yoshida, Y., Zhang, W., Zheng, B., Zhu, Q., Zhu, Q., and Zhuang, Q.: Global Methane Budget 2000–2020, Earth System Science Data, 17, 1873–1958, https://doi.org/10.5194/essd-17-1873-2025, 2025.

Schneising, O., Buchwitz, M., Reuter, M., Vanselow, S., Bovensmann, H., and Burrows, J. P.: Remote sensing of methane leakage from natural gas and petroleum systems revisited, Atmospheric Chemistry and Physics, 20, 9169–9182, https://doi.org/10.5194/acp-20-9169-2020, 2020.

Schuit, B. J., Maasakkers, J. D., Bijl, P., Mahapatra, G., van den Berg, A.-W., Pandey, S., Lorente, A., Borsdorff, T., Houweling, S., Varon, D. J., McKeever, J., Jervis, D., Girard, M., Irakulis-Loitxate, I., Gorroño, J., Guanter, L., Cusworth, D. H., and Aben, I.: Automated detection and monitoring of methane super-emitters using satellite data, Atmospheric Chemistry and Physics, 23, 9071–9098, https://doi.org/10.5194/acp-23-9071-2023, 2023.

Shen, L., Jacob, D. J., Gautam, R., Omara, M., Scarpelli, T. R., Lorente, A., Zavala-Araiza, D., Lu, X., Chen, Z., and Lin, J.: National quantifications of methane emissions from fuel exploitation using high resolution inversions of satellite observations, Nat Commun, 14, 4948, https://doi.org/10.1038/s41467-023-40671-6, 2023.

Sherwin, E. D., Rutherford, J. S., Zhang, Z., Chen, Y., Wetherley, E. B., Yakovlev, P. V., Berman, E. S. F., Jones, B. B., Cusworth, D. H., Thorpe, A. K., Ayasse, A. K., Duren, R. M., and Brandt, A. R.: US oil and gas system emissions from nearly one million aerial site measurements, Nature, 627, 328–334, https://doi.org/10.1038/s41586-024-07117-5, 2024.

Williams, J. P., Omara, M., Himmelberger, A., Zavala-Araiza, D., MacKay, K., Benmergui, J., Sargent, M., Wofsy, S. C., Hamburg, S. P., and Gautam, R.: Small emission sources in aggregate disproportionately account for a large majority of total methane emissions from the US oil and gas sector, Atmospheric Chemistry and Physics, 25, 1513–1532, https://doi.org/10.5194/acp-25-1513-2025, 2025.

Wolff, S., Ehret, G., Kiemle, C., Amediek, A., Quatrevalet, M., Wirth, M., and Fix, A.: Determination of the emission rates of CO_2 point sources with airborne lidar, Atmospheric Measurement Techniques, 14, 2717–2736, https://doi.org/10.5194/amt-14-2717-2021, 2021.

Zavala-Araiza, D., Alvarez, R. A., Lyon, D. R., Allen, D. T., Marchese, A. J., Zimmerle, D. J., and Hamburg, S. P.: Super-emitters in natural gas infrastructure are caused by abnormal process conditions, Nat Commun, 8, 14012, https://doi.org/10.1038/ncomms14012, 2017.